

Polarity-controllable magnetic skyrmion filter

Xiao-Lin Ai(艾啸林), Hui-Ting Li(李慧婷), Xue-Feng Zhang(张雪枫), Chang-Feng Li(李昌锋), Je-Ho Shim(沈帝虎), Xiao-Ping Ma(马晓萍), and Hong-Guang Piao(朴红光)

Citation :Chin. Phys. B, 2024, 33 (**10**): 107502. DOI: 10.1088/1674-1056/ad6421
Journal homepage: http://cpb.iphy.ac.cn; http://iopscience.iop.org/cpb

What follows is a list of articles you may be interested in

Dzyaloshinskii-Moriya interaction and field-free sub-10 nm topological magnetism in Fe/bismuth oxychalcogenides heterostructures

Yaoyuan Wang(王垚元), Long You(游龙), Kai Chang(常凯), and Hongxin Yang(杨洪新)
Chin. Phys. B, 2024, 33 (**9**): 097508. DOI: 10.1088/1674-1056/ad6a0e

Mapping the antiparallel aligned domain rotation by microwave excitation

Jing Zhang(张景), Yuanzhi Cui(崔远志), Xiaoyu Wang(王晓雨), Chuang Wang(王创), Mengchen Liu(刘梦晨), Jie Xu(徐洁), Kai Li(李凯), Yunhe Zhao(赵芸鹤), Zhenyan Lu(陆振烟), Lining Pan(潘丽宁), Chendong Jin(金晨东), Qingfang Liu(刘青芳), Jianbo Wang(王建波), and Derang Cao(曹德让)
Chin. Phys. B, 2024, 33 (**9**): 097506. DOI: 10.1088/1674-1056/ad5536

RKKY interaction in helical higher-order topological insulators

Sha Jin(金莎), Jian Li(李健), Qing-Xu Li(李清旭), and Jia-Ji Zhu(朱家骥)
Chin. Phys. B, 2024, 33 (**7**): 077503. DOI: 10.1088/1674-1056/ad3ef9

Oscillation of Dzyaloshinskii-Moriya interaction driven by weak electric fields

Runze Chen(陈润泽), Anni Cao(曹安妮), Xinran Wang(王馨苒), Yang Liu(柳洋), Hongxin Yang(杨洪新), and Weisheng Zhao(赵巍胜)
Chin. Phys. B, 2024, 33 (**2**): 027501. DOI: 10.1088/1674-1056/ad0f85

Progress on two-dimensional ferrovalley materials

Ping Li(李平), Bang Liu(刘邦), Shuai Chen(陈帅), Wei-Xi Zhang(张蔚曦), and Zhi-Xin Guo(郭志新)
Chin. Phys. B, 2024, 33 (**1**): 017505. DOI: 10.1088/1674-1056/acf65f

---

Polarity-controllable magnetic skyrmion filter

Xiao-Lin Ai(艾啸林)[1,†], Hui-Ting Li(李慧婷)[2,†], Xue-Feng Zhang(张雪枫)[2], Chang-Feng Li(李昌锋)[2], Je-Ho Shim(沈帝虎)[2,‡], Xiao-Ping Ma(马晓萍)[2], and Hong-Guang Piao(朴红光)[1,2,§]

[1] *Hubei Engineering Research Center of Weak Magnetic-Field Detection, College of Science, China Three Gorges University, Yichang* 443002, *China*
[2] *Department of Physics, College of Science, Yanbian University, Yanji* 133002, *China*

(Received 19 May 2024; revised manuscript received 9 July 2024; accepted manuscript online 17 July 2024)

The skyrmion generator is one of the indispensable components for the future functional skyrmion devices, but the process of generating skyrmion cannot avoid mixing with other magnetic textures, such as skyrmionium and nested skyrmion bags. These mixed magnetic textures will inevitably lead to the blockage of skyrmion transport and even the distortion of data information. Therefore, the design of an efficient skyrmion filter is of great significance for the development of skyrmion-based spintronic devices. In this work, a skyrmion filter scheme is proposed, and the high-efficiency filtering function is demonstrated by micromagnetic simulations. The results show that the filtering effect of the scheme depends on the structure geometry and the spin current density that drives the skyrmion. Based on this scheme, the polarity of the filtered skyrmion can be controlled by switching the magnetization state at the output end, and the "cloning" of the skyrmion can be realized by geometric optimization of the structure. We believe that in the near future, the skyrmion filter will become one of the important components of skyrmion-based spintronic devices in the future.

Keywords: spintronics, skyrmions, skyrmion filter, skyrmion polarity, skyrmion clone

PACS: 75.47.–m, 12.39.Dc, 75.78.Cd **DOI:** 10.1088/1674-1056/ad6421

1. Introduction

Magnetic skyrmion, a type of spin texture with topological property, have been experimentally confirmed to exist in B20 transition metal compounds with non-centrosymmetric crystal structures.[1] Skyrmion is considered to be the most competitive information carrier in the next generation of magnetic memories and logic devices[1–7] due to its stable topological magnetic structure, extremely small size (3 nm–100 nm), and low threshold operating current density ($\sim 10^6$ A/m^2). In recent years, the upsurge of research on magnetic skyrmion[8–20] has actively promoted the rapid development of related fields of spintronics.[1–7,21–24]

However, since there are other members of the skyrmion family such as anti-skyrmion,[25] skyrmionium,[26] and nested skyrmion bags,[26,27] a stable source or filter that can provide pure skyrmion is required for future skyrmion-based magnetic memories and logic devices. At present, skyrmion and other members can be created in magnetic thin film materials with Dzyaloshinskii–Moriya interaction (DMI)[28–31] by various technical methods of spin-polarized current,[13,32,33] optical laser,[12,34] and magnetic field.[35] However, since these methods cannot precisely control the local energy, they inevitably result in transformation between skyrmion and other skyrmion members, and even with other topological spin textures. For example, for the case of spin-polarized current, skyrmion can be created near the 10^8-A/cm^2 current density, but skyrmion is replaced by other spin textures once this range is exceeded.[14] For cases of the optical laser[12] or magnetic field,[36] the transformation between skyrmions and other skyrmion members can also be caused by controlling the action energy. In addition, the existence of various defects in the same sample under the same conditions may affect creation of skyrmion.[37] If other skyrmion family members are mixed into the skyrmion-based magnetic memories or logic devices, the consequences are unimaginable, which would inevitably cause information distortion and data confusion. Therefore, it is necessary to design a skyrmion filter between the skyrmion source component and the functional component in the skyrmion-based devices to ensure the injection of pure skyrmion flow.

In recent years, effective methods for purifying skyrmion have been reported, which can be roughly divided into two methods: one is a dynamic separation method based on Magnus force,[38] and the other is a reconstruction method based on spin structure transformation. For the first method, since the magnitude and direction of Magnus force mainly depend on the topological characteristics of the spin structure, members of the skyrmion family are affected by the Magnus force differently under the same conditions, and present different dynamic responses and motion paths.[39,40] However, although the Magnus force method can realize the selective filtering of skyrmion by designing special geometry, it is difficult to realize due to the strict technical requirements on micro-machining, material preparation and electrical con-

[†]These authors contributed equally to this work.
[‡]Corresponding author. E-mail: shendihu@gmail.com
[§]Corresponding author. E-mail: hgpiao@ybu.edu.cn

© 2024 Chinese Physical Society and IOP Publishing Ltd

trol technology.[41] For the second method, the topological spin structure can be reconstructed by external field, which can realize the purification of spin textures. For examples, the transformation between meron and skyrmion,[42] skyrmion and anti-skyrmion,[43] and skyrmion and skyrmionium[44] can be achieved through external field modulation. In addition, the dependence of spin texture on the geometry of ferromagnetic nanostructures can be exploited to allow the members of the skyrmion family to convert into multiple magnetic domain walls when passing through the nanowire structure,[15,45] and conversely to convert the magnetic domain walls (DWs) into pure skyrmions.

In the present study, a filtering behavior of skyrmions will be investigated in patterned ferromagnetic nanowires (skyrmion filters), which utilizes the spin structure transformation between DWs and the skyrmion family members dependent on the geometry of ferromagnetic nanostructures. The basic structure of the skyrmion filter is mainly composed of three parts, such as input pad, channel, and output pad, as shown in Fig. 1(a).

Here, a swallowtail structure was designed at the right end of input pad, to prevent skyrmions from colliding with the nanowire ends and annihilating. To prevent the DWs from not easily reconstructing skyrmions due to the adsorption effect at the nanowire ends, the swallowtail structure was also designed at the left end of output pad. In order to make the spin textures of the skyrmion family easily converted into a spatially confined magnetic domain (MD), the channel is designed as a narrow nanowire structure. Two cases are considered in this paper, one is the case A where the input and output magnetization directions are the same (see Fig. 1(a)), the other is the case B where the magnetization is in the opposite direction (see Fig. 1(b)).

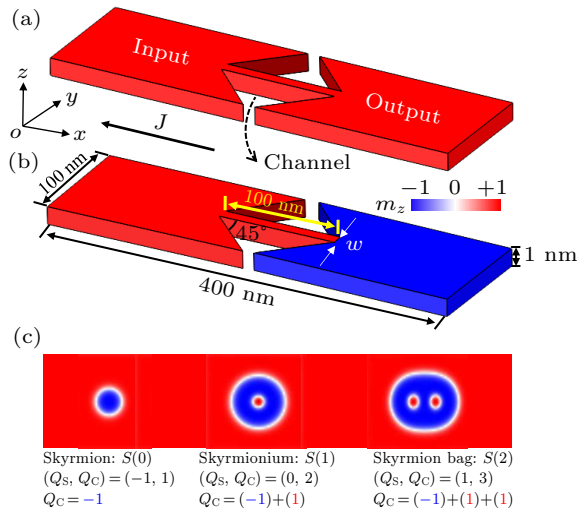


Fig. 1. (a) Schematic diagram of a skyrmion filter when the input and output pads have same polarities. (b) Schematic diagram of a skyrmion filter when the input and output pads have opposite polarities. (c) Topological properties of skyrmion family members $S(n)$. (n: number of inner skyrmions, Q_S: topological total degree, Q_C: topological cumulative number).

2. Micromagnetic simulations

In order to demonstrate the effectiveness of the designed basic structures on the filtering behavior of skyrmions, the micromagnetic simulations were performed by using the MuMax3 software.[46] In the basic structure of the skyrmion filter, the total space size is set to 400 nm×100 nm×1 nm with the cell size of 2 nm×2 nm×1 nm. The geometrical parameters are represented in the Fig. 1(b), the angle of the swallowtail structure and the channel is set to 45°, the channel length is 100 nm, and effective space scales of the input and output pads are 150 nm×100 nm×1 nm. Here, the channel width (w) is varied in the range of 8 nm to 20 nm considering the skyrmion diameter. Material parameters of the Co/Pt material[14,47,48] are used as follows: the saturation magnetization $M_s = 580$ kA/m, the perpendicular magnetic anisotropy (PMA) constant $K_u = 0.8$ MJ/m^3, DMI constant $D = 3.5$ mJ/m^2, Heisenberg exchange stiffness $A = 15$ pJ/m, and the Gilbert damping constant $\alpha = 0.3$. In all the simulations, the skyrmions in the patterned nanostructure are driven along the x-axis direction by spin-polarized currents with the current density of $J = 8 \times 10^{12}$ A/m^2 $\sim 22 \times 10^{12}$ A/m^2, the polarization rate $P = 0.4$,[14] and the non-adiabatic torque coefficient $\beta = 0.3$.[1] For the sake of discussion, it is necessary to establish a standardized system for the members of the skyrmion family, such as Eq. (1),

$$\begin{aligned} &\text{Type of skyrmion members: } S(n) \\ &Q_S(n) = \pm(n-1), \quad Q_C(n) = n+1. \end{aligned} \tag{1}$$

Here, $S(n)$ means that a skyrmion member has n inner skyrmions, and $Q_C(n)$ is a topological total number (or topological total degree).[26] $Q_S(n)$ is a topological cumulative number, that is the sum of the number of skyrmion structures within $S(n)$, which means the maximum number of skyrmions that can be formed if the $S(n)$ splits. As shown in Fig. 1(c), three skyrmion family members are used in this work, such as skyrmion $S(0)$, skyrmionium $S(1)$, and nested skyrmion bag with two inner skyrmions $S(2)$.

3. Results and discussion

To investigate the filtering effect of the basic structure on skyrmions, the $S(0)$ and $S(1)$ are initially set in the input pad for the case A, and they are passed through the channel ($w = 10$ nm) to the output pad under the driving electrical current of $J = 21 \times 10^{12}$ A/m^2, as shown in Fig. 2. Since the $Q_C(n)$ sum of $S(0)$ and $S(1)$ is $Q_C(0) + Q_C(1) = 3$, three skyrmions can be formed in the output pad after filtering.

As shown in the top of Fig. 2(a), the time-varying law of exchange energy and demagnetization energy is observed during the whole process of $S(0)$ and $S(1)$ reconstituted to skyrmions in the output pad after channel filtering. It was found that $S(0)$ and $S(1)$ were transformed to three MDs by

the channel in three steps of I, II, and III (see three red areas of steep ascent), and then reconstructed to three skyrmions through three steps of IV, V, and VI (see three blue areas of slow descent). Here, the steep ascent means crossing an energy barrier, and the slow descent means entering an energy well. This indicates that the skyrmion topological structure in the system is relatively stable in energy compared to the DW structure. As shown in left of Fig. 2(b), it is observed that all shells (including the inner shells) of $S(0)$ and $S(1)$ are transformed to DWs in the steps I, II, and III when they encounter the channel. From the step I, it can be observed that the left and right shells of $S(0)$ transform to the DWs on both sides of the blue MD in the channel respectively, and the MD continues to advance towards the output pad under the current drive. In the steps II and III, the $S(1)$ is transformed to three adjacent MDs (2 blue and 1 red) with four DWs because it has two shells of outer and inner. As the green arrows as shown in the down of Fig. 2(a), the energy change rate is the most dramatic, every time the skyrmion shell transforms into a DW, which also means that there is a barrier between the two structures, such as a barrier caused by the repulsive force of the structure edge on the skyrmions[20] or a topological skyrmion energy barrier.[49] In addition, it is also observed that when each MD is reconstituted to the skyrmion in the output pad after filtering, its energy decreases slowly and even the energy change rate appears a valley value (see black arrows) when each DW is transformed to the skyrmion shell, as the IV, V, and VI blue areas shown in Fig. 2(a). This further confirms that the energy state of the skyrmion structure is more stable than that of the DW. Interestingly, for the case B, the filter can output skyrmions with opposite polarity, as shown in Fig. 3. This means that our designed skyrmion filter can be applied to functional devices that utilize different polars of the skyrmion.

In order to verify the influence of the drive current and the channel geometry on the skyrmion filtering effect, the number of skyrmions effectively formed in the output pad was analyzed by changing the drive current density ($J = 8\times10^{12}$ A/m^2 $\sim$ 22×10^{12} A/m^2 and channel width ($w =$ 8 nm$\sim$20 nm), and color maps reflecting the filtering effect were drawn for the A and B cases respectively, as shown in Fig. 4. In both cases, it is clearly seen that the skyrmion filtering effect is easily affected by the drive current density and the channel geometry. For case A, it can be observed that when the channel width or drive current density is too small, the filter action of the device is less stable. Although there is a certain complementary relationship between the channel width and the drive current density, if the channel width is too small ($w \leq 12$ nm) for the skyrmion to pass through, and if the current density is too small ($J = 10\times10^{12}$ A/m^2) for the skyrmion to overcome the energy barrier and move forward (see blue areas). In case B, the complementary relationship between the channel width and the drive current density is generally similar to that in case A, as show in Fig. 4(b). However, there is a new phenomenon in case B that cannot appear in case A, that is, the output pad magnetization reversal phenomenon, as shown in the inset of Fig. 4(b). The phenomenon mainly appears in the wider channel and larger current density conditions, refer to the distortion region (white areas) shown in Fig. 4(b). Nevertheless, we prove that the proposed skyrmion filter scheme is effective and feasible within a certain range of channel size and drive current density.

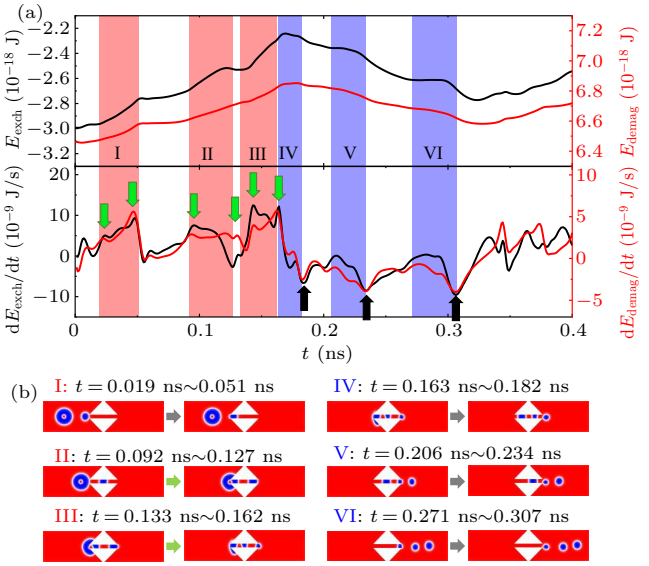


Fig. 2. The case A when a skyrmion family member of $S(0)+S(1)$ is entered into the input pad. Channel width is 10 nm and driving electrical current of $J = 21\times10^{12}$ A/m^2. Input and output pads have same polarities. (a) Top: Time versus exchange energy E_{exch} (black), and time versus demagnetization energy E_{demag} (red). Bottom: Time versus rate of change of energy per second. Processes I, II, III: The process in which skyrmions in the input pad are injected into the channel and converted into magnetic domains (MDs). Processes IV, V, VI: The process in which MDs in the channel are injected into the output pad and converted to skyrmions. (b) Snapshots of each process (I–VI).

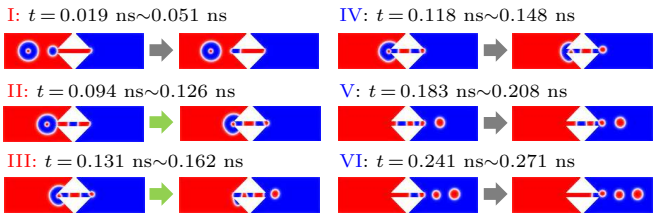


Fig. 3. Snapshots of each process (I–VI) in case B. Input and output pads have opposite polarities. The case B when a skyrmion family member of $S(0)+S(1)$ is entered into the input gate. Channel width is 10 nm and driving electrical current of $J = 21\times10^{12}$ A/m^2.

In order to demonstrate the extensibility of this skyrmion filter, we designed a Y-shaped dual-output mode structure with the same magnetization and opposite magnetization states, as shown in Figs. 5(a) and 5(b). Moreover, to further confirm that this filter design is also effective for other members of the skyrmion family, one skyrmion $S(0)$ and one nested skyrmion bag $S(2)$ are initially set in the input pad, and its filtering effect is investigated by simulations with the channel $w = 14$ nm

under $J = 13 \times 10^{12}$ A/m^2. The dimensions of the dual-output filter are described in detail in the top of Fig. 5(a). The filter mechanism of the two-output mode structure is similar to that of the basic structure (see Fig. 2), but its Y-channel structure gives it an additional function of DW "cloning", thus filtering out double skyrmion in the dual-output pad, as shown in Fig. 5(a). More interestingly, if the magnetization of the dual-output pad is in the opposite state, it can output the same number of skyrmions with different polarity in their respective output pads despite some time difference, as shown in Fig. 5(b).

In order to further prove the feasibility and application value of this "clone" filter structure design, the relationship between the number of channels in this filter structure and the maximum number of skyrmions output after filtering ($N_{\mathrm{SK}}^{\max}$) is analyzed through a large number of simulations. As shown in Fig. 5(d), There is a linear relationship between the number of channels and the maximum number in the different total topological cumulative number cases of P$_1$: $\sum_i (Q_{\mathrm{C}}(n))_i = 3$, P$_2$: $\sum_i (Q_{\mathrm{C}}(n))_i = 4$, and P$_3$: $\sum_i (Q_{\mathrm{C}}(n))_i = 6$, and obey the following relationship:

$$N_{\mathrm{SK}}^{\max} = \left[\sum_i (Q_{\mathrm{C}}(n))_i\right] \times N_{\mathrm{out}}, \tag{2}$$

where N_{out} is the number of output pads, the i refers to the i-th skyrmion of the input pad. More interestingly, we found that for Néel-type and Bloch-type skyrmions, the numerical relationship of the cloning efficiency conforms to Eq. (2), and the cloned skyrmions remain the original Néel-type or Bloch-type. The results show that the cloning effect of skyrmions mainly depends on the DMI properties of the material, that is, the interfacial DMI is easy to form Néel-type skyrmion and the bulk DMI is easy to form Bloch-type.[50,51]

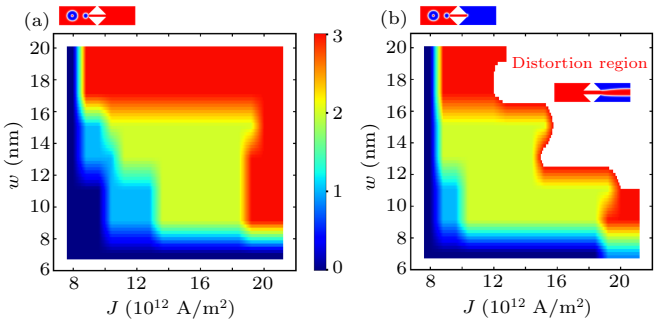


Fig. 4. Skyrmion filtering number diagram dependent on filtering channel width w and current density J. The region with different colors represents the skyrmion filtering number in the output pad is 3, 2, 1, and 0, respectively. (a) Skyrmion filtering number diagram of case A. It can be observed that when the channel width or drive current density is too small, the filter action of the device is less stable, refer to blue areas. (b) Skyrmion filtering number diagram of case B. The distortion region (white areas) indicates the output pad magnetization reversal by over currents.

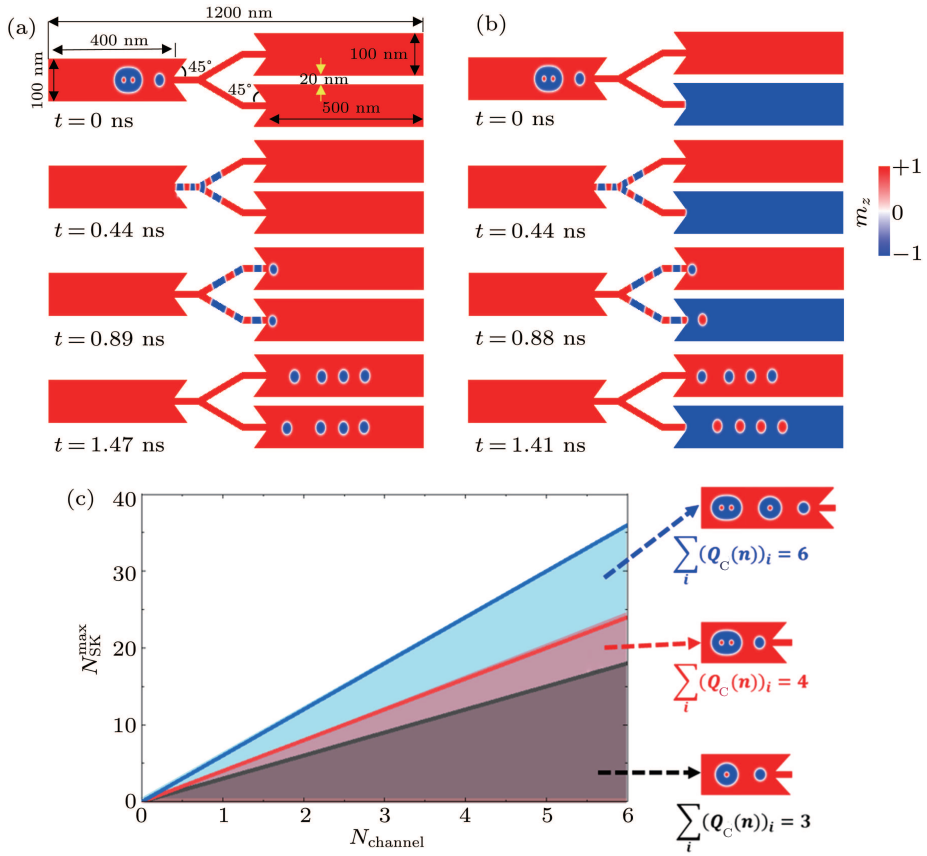


Fig. 5. (a) Snapshot of the magnetization state of the Y-shaped dual-output mode structure over time when the channel width is 14 nm, $J = 13 \times 10^{12}$ A/m^2, and the input pad and output pads have the same polarity. (b) Snapshot of the magnetization state of the Y-shaped dual-output mode structure over time under the same conditions as panel (a), except that the polarities of the input and output pads are opposite. (c) Number of channels N_{channel} versus maximum number of filtering skyrmions $N_{\mathrm{SK}}^{\max}$. The $N_{\mathrm{SK}}^{\max}$ depends on total topological cumulative number in input pad $\sum_i (Q_{\mathrm{C}}(n))_i$. Black, red, and blue lines are case of P$_1$ ($\sum_i (Q_{\mathrm{C}}(n))_i = 3$), P$_2$ ($\sum_i (Q_{\mathrm{C}}(n))_i = 4$), and P$_3$ ($\sum_i (Q_{\mathrm{C}}(n))_i = 6$).

4. Conclusion

In summary, we have designed a skyrmion filter with the function of controlling polarity and "cloning" DW, which can effectively filter out any number of pure skyrmions with different polarity. Although our design scheme is not perfect yet, with the development of experimental preparation technology,[52] our design ideas will provide references for the design and application of spintronic devices.

Acknowledgements

Project supported by the National Natural Science Foundation of China (Grant No. 12364020), the Scientific and Technological Development Plan of Jilin Province, China (Grant No. 20240101295JC), the Science and Technology Research and Planning Project of Jilin Provincial Department of Education (Grant No. JJKH20230611KJ), and the Applied Foundation Research Project (Talent Funding Project) of Yanbian University (Grant No. ydkj202241).

References

[1] Mühlbauer S, Binz B, Jonietz F, Pfleiderer C, Rosch A, Neubauer A, Georgii R and Böni P 2009 *Science* **323** 915
[2] Zhang X, Ezawa M and Zhou Y 2015 *Sci. Rep.* **5** 9400
[3] Luo S, Song M, Li X, Zhang Y, Hong J, Yang X, Zou X, Xu N and You L 2018 *Nano Lett.* **18** 1180
[4] Yan Z R, Liu Y Z, Guang Y, Yue K, Feng J F, Lake R K, Yu G Q and Han X F 2021 *Phys. Rev. Appl.* **15** 064004
[5] Luo S and You L 2021 *APL Mater.* **9** 050901
[6] Zhang H, Zhu D, Kang W, Zhang Y and Zhao W 2020 *Phys. Rev. Appl.* **13** 054049
[7] Kang W, Zheng C, Huang Y, Zhang X, Zhou Y, Lv W and Zhao W 2016 *IEEE Electron Dev. Lett.* **37** 924
[8] Woo S, Litzius K, Krüger B, Im M Y, Caretta L, Richter K, Mann M, Krone A, Reeve R M, Weigand M, Agrawal P, Lemesh I, Mawass M A, Fischer P, Kläui M and Beach G S D 2016 *Nat. Mater.* **15** 501
[9] Das S, Tang Y L, Hong Z, Gonçalves M A P, McCarter M R, Klewe C, Nguyen K X, Gómez-Ortiz F, Shafer P, Arenholz E, Stoica V A, Hsu S L, Wang B, Ophus C, Liu J F, Nelson C T, Saremi S, Prasad B, Mei A B, Schlom D G, Íñiguez J, García-Fernández P, Muller D A, Chen L Q, Junquera J, Martin L W and Ramesh R 2019 *Nature* **568** 368
[10] Miao B F, Sun L, Wu Y W, Tao X D, Xiong X, Wen Y, Cao R X, Wang P, Wu D, Zhan Q F, You B, Du J, Li R W and Ding H F 2014 *Phys. Rev. B* **90** 174411
[11] Yu X Z, Onose Y, Kanazawa N, Park J H, Han J H, Matsui Y, Nagaosa N and Tokura Y 2010 *Nature* **465** 901
[12] Finazzi M, Savoini M, Khorsand A R, Tsukamoto A, Itoh A, Duò L, Kirilyuk A, Rasing T and Ezawa M 2013 *Phys. Rev. Lett.* **110** 177205
[13] Romming N, Hanneken C, Menzel M, Bickel J E, Wolter B, Bergmann K V, Kubetzka A and Wiesendanger R 2013 *Science* **341** 636
[14] Sampaio J, Cros V, Rohart S, Thiaville A and Fert A 2013 *Nat. Nanotechnol.* **8** 839
[15] Jiang W, Upadhyaya P, Zhang W, Yu G, Jungfleisch M B, Fradin F Y, Pearson J E, Tserkovnyak Y, Wang K L, Heinonen O, Velthuis S G E T and Hoffmann A 2015 *Science* **349** 283
[16] Rohart S and Thiaville A 2013 *Phys. Rev. B* **88** 184422
[17] Komineas S and Papanicolaou N 2015 *Phys. Rev. B* **92** 174405
[18] Komineas S and Papanicolaou N 2015 *Phys. Rev. B* **92** 064412
[19] Iwasaki J, Koshibae W and Nagaosa N 2014 *Nano Lett.* **14** 4432
[20] Ma X P, Ai X, Yang X X, Cai M X, Shim J H and Piao H G 2023 *J. Magn. Magn. Mater.* **581** 170665
[21] Zhang X, Zhao G, Fangohr H, Liu J P, Xia W X, Xia J and Morvan F J 2015 *Sci. Rep.* **5** 7643
[22] Zhang X, Zhou Y, Ezawa M, Zhao G P and Zhao W 2015 *Sci. Rep.* **5** 11369
[23] Liang X, Zhang X, Xia J, Ezawa M, Zhao Y, Zhao G and Zhou Y 2020 *Appl. Phys. Lett.* **116** 122402
[24] Zhu D, Kang W, Li S, Huang Y, Zhang X, Zhou Y and Zhao W 2017 *IEEE. T. Electron. Dev.* **65** 87
[25] Nayak A K, Kumar V, Ma T, Werner P, Pippel E, Sahoo R, Damay F, Rößler U K, Felser C and Parkin S S P 2017 *Nature* **548** 561
[26] Foster D, Kind C, Ackerman P J, Tai J S B, Dennis M R and Samlyukh I I 2019 *Nat. Phys.* **15** 655
[27] Kind C and Foster D 2021 *Phys. Rev. B* **103** L100413
[28] Hog S E, Bailly-Reyre A and Diep H T 2018 *J. Magn. Magn. Mater.* **455** 32
[29] Yang H, Chen G, Cotta A A C, N'Diaye A T, Nikolaev S A, Soares E A, Macedo W A A, Liu K, Schmid A K, Fert A and Chshiev M 2018 *Nat. Mater.* **17** 605
[30] Yang H, Liang J and Cui Q 2023 *Nat. Rev. Phys.* **5** 43
[31] Yang H, Thiaville A, Rohart S, Fert A and Chshiev M 2015 *Phys. Rev. Lett.* **115** 267210
[32] Yuan H Y and Wang X R 2016 *Sci. Rep.* **6** 22638
[33] Everschor-Sitte K, Sitte M, Valet T, Abanov A and Sinova J 2017 *New J. Phys.* **19** 092001
[34] Koshibae W and Nagaosa N 2016 *Nat. Commun.* **5** 5148
[35] Moreau-Luchaire C, Moutafis C, Reyren N, Sampaio J, Vaz C A F, Horne N V, Bouzehouane K, Garcia K, Deranlot C, Warnicke P, Wohiüter P, George J-M, Weigand M, Raabe J, Cros V and Fert A 2016 *Nat. Nanotech.* **11** 444
[36] Zhang X, Xia J, Zhou Y, Wang D, Liu X, Zhao W and Ezawa M 2016 *Phys. Rev. B* **94** 094420
[37] Ran N, Zhao G P, Tang H, Shen L C, Lai P, Xia J, Zhang X and Zhou Y 2017 *AIP Adv.* **7** 025105
[38] Brown B L, Täuber U C and Pleimling M 2018 *Phys. Rev. B* **97** 020405
[39] Chen R and Li Y 2022 *ACS Appl. Mater. Interfaces* **14** 30420
[40] Li L, Luo J, Xia J, Zhou Y, Liu X and Zhao G 2023 *Chin. Phys. B* **32** 017506
[41] Shen L, Li X, Zhao Y, Xia J, Zhao G and Zhou Y 2019 *Phys. Rev. Appl.* **12** 064033
[42] Yu X Z, Koshibae W, Tokunaga Y, Shibata K, Taguchi Y, Nagaosa N and Tokura Y 2018 *Nature* **564** 95
[43] Peng L, Takagi R, Koshibae W, Shibata K, Nakajima K, Arima T H, Nagaosa N, Seki S, Yu X and Tokura Y 2020 *Nat. Nanotechnol.* **15** 181
[44] Yang S, Zhao Y, Wu K, Chu Z, Xu X, Li X, Åkerman J and Zhou Y 2023 *Nat. Commun.* **14** 3406
[45] Zhou Y and Ezawa M 2014 *Nat. Commun.* **5** 4652
[46] Vansteenkiste A, Leliaert J, Dvornik M, Helsen M, Garcia-Sanchez F and Waeyenberge B V 2014 *AIP Adv.* **4** 107133
[47] Fert A, Cros V and Sampaio J 2013 *Nat. Nanotechnol.* **8** 152
[48] Metaxas P J, Jamet J P, Mougin A, Cormier M, Ferré J, Baltz V, Rodmacq B, Dieny B and Stamps R L 2007 *Phys. Rev. Lett.* **99** 217208
[49] Leishman A W D, Menezes R M, Longbons G, Bauer E D, Janoschek M, Honecker D, DeBeer-Schmitt L, White J S, Sokolova A, Milošević M V and Eskildsen M R 2020 *Phys. Rev. B* **102** 104416
[50] Everschor-Sitte K, Masell J, Reeve R M and Kläui M 2018 *J. Appl. Phys.* **124** 240901
[51] Du H and Wang X 2022 *Chin. Phys. B* **31** 087507
[52] Liu J, Wang Z, Xu T, Zhou H, Zhao L, Je S, Im M, Fang L and Jiang W 2022 *Chin. Phys. Lett.* **39** 017501